https://doi.org/10.15407/ufm.22.04.481

A.M. GUSAK* and N.V. STOROZHUK**
The Bohdan Khmelnytsky National University of Cherkasy,
81 Shevchenko Blvd., UA-18031 Cherkasy, Ukraine
*amgusak@ukr.net, **nadushenka@ukr.net

MODELLING OF PHASE FORMATION IN SOLID–SOLID AND SOLID–LIQUID INTERACTIONS: NEW DEVELOPMENTS

Recent developments (after 2016) in modelling of phase formation during solid–solid and solid–liquid reactions by SKMF (Stochastic Kinetic Mean-Field) method, Monte Carlo simulation and phenomenological modelling are reviewed. Reasonable results of multiphase reactive diffusion modelling demonstrating distinct concentration plateau for each intermediate ordered compound and distinct concentration steps between these phases are obtained by the SKMF and Monte Carlo methods, if one takes into account interatomic interactions within two coordination shells and if the signs of mixing energies are 'minus' for the first coordination shell and 'plus' for the second one. Second possibility for reasonable modelling results is consideration of interatomic interactions depending on local concentration with maxima around stoichiometric composition. In phenomenological modelling, the generalization of Wagner diffusivity concept and respective superposition rule are introduced. New mechanism of the lateral grain growth in the growing phase layers during reactive diffusion is suggested. Anomalously fast grain growth at the final stages of soldering in sandwich-like Cu–Sn–Cu contacts is reported and explained. Simple model of Zn-additions' influence on the Cu–Sn reaction is described.

Keywords: interdiffusion, intermediate phases, ordering, modelling, mean-field approximation, noise, Monte Carlo method, soldering

1. Introduction

Reactive diffusion is a process of interdiffusion (when both reagents are in condensed state) or one-side diffusion (if one of reagents penetrates into condensed phase from the gas phase) accompanied by the formation, growth and (in many cases) competition of chemical compounds

Citation: A.M. Gusak and N.V. Storozhuk, Modelling of Phase Formation in Solid–Solid and Solid–Liquid Interactions: New Developments, *Progress in Physics of Metals*, **22**, No. 4: 481–510 (2021)

which in most cases are in fact the ordered intermediate phases. Reactive diffusion controls such important processes as soldering [1], brazing, SHS and 3*D*-printing [2, 3], silicide formation in the integral circuits [4], at the point contacts of nanowires [5], sintering of binary and multicomponent powders [6] etc. Our present topic, in short, is modelling (by various methods) of reactive diffusion. We mean the new results obtained during last few years, after the reviews [7, 8].

'Solid-state reactions' is a chemical term, but we will treat these reactions from the physical point of view. For physicist, reaction in the contact zone of two materials is a phase transformation in an open inhomogeneous system. It includes nucleation, ordering, growth, coarsening of new phases in the sharp concentration gradients, which decrease with time. Action of sharp concentration gradient is in some sense analogical to high cooling rate [9]: High cooling rate (quenching) may suppress partially or practically all phase transformations. Sufficiently sharp concentration gradient also may suppress partially or practically all intermediate phase formations; this was demonstrated earlier in collaboration with Pierre Desre and Fiqiri Hodaj [10–15].

Despite big progress in understanding of solid-state reactions, many problems still remain unsolved (choice of reaction path in multiphase system, interdependence of grain-structure evolution and reaction kinetics during reactive diffusion, influence of third component on the product and kinetics of solid-state reactions, voiding during reactive diffusion, phase competition in SHS reactions etc.)

We will discuss some new results on solid-state reactions modelling obtained after 2016 by 3 methods — (1) stochastic kinetic mean-field method, (2) Monte Carlo, and (3) phenomenological modelling.

2. Modelling of Solid-State Reactions by Kinetic Mean-Field Method with Stochastic Additions

Since 2014 our group, jointly with the group of Professor Erdelyi, has been developing the so-called Stochastic Kinetic Mean-Field method (further below SKMF), which is, we would say, not a new method but a new version, new development of non-linear Kinetic Mean-Field method (further below KMF) suggested in 1990 by George Martin [16–23]. In 2013, we generalized the quasi-one-dimensional Martin's method on 3*D*-case [18]. The main equations are, in fact, the master equations for the probabilities of any site to be occupied by sort A or B (we shortly call these probabilities 'concentrations'). In the simplest case of exchange mechanism within the first coordination shell, these equations are following:

$$\frac{dC_A[i]}{dt} = \sum_{in=1}^{Z} \left(-C_A[i]C_B[in]\,\Gamma[i(A), in(B)] + \right.$$
$$\left. + C_B[i]C_A[in]\,\Gamma[in(A), i(B)]\right). \qquad (1)$$

Change rate of these concentrations are determined by the transition frequencies, which exponentially depend on the energy change during transition, and energies, in their turn, linearly depend on concentrations:

$$\begin{aligned}\Gamma[i(A), in(B)] &= \nu_0 \exp\left(-\frac{Q_{i,in}}{kT}\right) = \\ &= \nu_0 \exp\left(-\frac{E^s - \left(E_A[i] + E_B[in]\right)}{kT}\right),\end{aligned} \tag{2}$$

$$E_A[i] = \sum_{in=1}^{Z} \left(C_A[in] \cdot V_{AA} + C_B[in] \cdot V_{AB}\right). \tag{3a}$$

$$E_B[in] = \sum_{inn=1}^{Z} \left(C_A[inn] \cdot V_{BA} + C_B[inn] \cdot V_{BB}\right). \tag{3b}$$

We remind that the energies in these equations are the expectation (mean) values of interaction energies with neighbours obtained under neglecting of correlations (for example, here, $C_A[in]$ is a probability of neighbouring site 'in' to be occupied by sort A even if the probability of site 'i' to be occupied also by sort A is unity) — this is exactly the basic simplification in mean-field models.

If we put time derivatives in eq. (1) to be zero, we get steady-state condition, which, in closed system, means equilibrium:

$$C_A[i] C_B[in]\, \Gamma[i(A), in(B)] = C_B[i] C_A[in]\, \Gamma[in(A), i(B)], \tag{4}$$

or, in other form,

$$\frac{C_A[i]}{C_B[i]} \exp\left(\frac{E_A[i] - E_B[i]}{kT}\right) = \frac{C_A[in]}{C_B[in]} \exp\left(\frac{E_A[in] - E_B[in]}{kT}\right). \tag{5}$$

From thermodynamic point of view, equilibrium means constant chemical potentials of any component. If one takes the logarithm of eq. (5), one gets the constant value of reduced chemical potential in all sites:

$$\begin{aligned}\tilde{\mu}[i] &= \mu_A[i] - \mu_B[i] = kT \ln \frac{C_A[i]}{C_B[i]} + E_A[i] - E_B[i] = \\ &= kT \ln \frac{C_A[i]}{C_B[i]} - 2V_{mix} \sum_{in=1}^{Z} C_A[in] + Z \cdot \left(V_{AB} - V_{BB}\right).\end{aligned} \tag{6}$$

Thus, comparison of two approaches gives quite realistic atomistic treatment of reduced chemical potential (change of Gibbs free energy due to replacement of atom B by atom A) in terms of occupation probabilities and interaction energies. Condition of steady-state with constraint of constant reduced chemical potential provides the nonlinear equation for determining the long-range order, coinciding with Khachaturyan's equations [24], obtained by him in the frame of concentration

waves method:

$$C_A[i] = \left(1 - C_A[i]\right)\exp\left(\frac{2V_{mix}}{kT}\sum_{in=1}^{Z} C_A[in]\right)\exp\left(\frac{\tilde{\mu} - Z\cdot\left(V_{AB} - V_{BB}\right)}{kT}\right). \quad (7)$$

Reduced chemical potential in eq. (7) is found from the constraint

$$\sum_{i=1}^{N} C_A[i] = N\bar{C}_A\,. \quad (8)$$

We proved that the change rate of Gibbs free energy of the system can be expressed in the form of sum containing only positive summands and global 'minus' [21,22]:

$$\frac{dG}{dt} = -\nu_0 \exp\left(-\frac{E^s}{kT}\right)\times$$

$$\times \sum_{(i,in)}^{NZ/2}\left[C_B[i]C_B[in]\exp\left(\frac{E_B[i] + E_B[in]}{kT}\right)\left(\tilde{\mu}_{AB}[i] - \tilde{\mu}_{AB}[in]\right)\times\right. \quad (9)$$

$$\left.\times\left(\exp\left(\frac{\tilde{\mu}_{AB}[i]}{kT}\right) - \exp\left(\frac{\tilde{\mu}_{AB}[in]}{kT}\right)\right)\right],$$

$$\left.\frac{dG}{dt}\right|_{KMF} \le 0\,(= 0 \text{ at equilibrium})\,. \quad (10)$$

Mathematically, the proof in [21, 22] is very similar to the proof of Boltzmann's H-theorem for entropy evolution. So, we rigorously proved that the Kinetic Mean Field model may describe only relaxation processes without any overcoming of energetic barriers. Thus, KMF cannot describe the first-order phase transformations, including the nucleation stage.

To describe the overcoming of nucleation barrier, one has to introduce some noise. The usual way of introducing noise of the Langevin type is the random additions to the probabilities (concentrations) and to the local order parameter [25]. In our case, due to strictly positive (and less than unit) nature of probabilities, and due to matter conservation, we prefer to introduce noise to transition frequencies (in other words, to the atom-range fluxes between neighbouring sites). For simplicity, we treat this noise of frequencies as a white noise, without any time correlations. Moreover, in our case we do not need any additional long-range order (LRO) parameter since concentrations/probabilities are introduced at the atomic scale and they determine automatically the local order parameter for every site according to standard definition of order applied to finite atomic clusters. Thus, our KMF scheme was modified in the following manner:

$$\frac{dC_i}{dt} = -\sum_{j=1}^{Z}\left[C_i(1 - C_j)\left(\Gamma_{i,j} + \delta\Gamma_{i,j}^{Lang}\right) - (1 - C_i)\,C_j\left(\Gamma_{j,i} + \delta\Gamma_{j,i}^{Lang}\right)\right], \quad (11)$$

$$\delta\Gamma_{i,k}^{Lang} = \frac{A_n}{\sqrt{dt}}\sqrt{3}\left(2\cdot random - 1\right), \tag{12}$$

$$< \delta\Gamma_{i,j}^{Lang}(t)\,\delta\Gamma_{k,m}^{Lang}(t') >= A_n^2\delta_{ik}\delta_{jm}\delta(t-t'). \tag{13}$$

If one uses standard mean-field approximation with account of only nearest neighbours interactions (within the first coordination shell), one gets the following dependence of Gibbs free energy per atom on temperature, on concentration, and on local order for solid solution and for the ordered f.c.c. phases $L1_2$ and $L1_0$:

$$g^{disordered} = 6\left(C_A V_{AA} + C_B V_{VV}\right) + 12 C_A C_B V_{mix} + kT\left(C_A \ln C_A + C_B \ln C_B\right), \tag{14}$$

$$\begin{aligned} g^{L1_0} &= 6\left(C_A V_{AA} + C_B V_{BB}\right) + 12 C_A C_B V_{mix} + V_{mix}\eta^2 + \\ &+ \frac{kT}{2}\left(\begin{array}{l}\left(C_A + \frac{\eta}{2}\right)\ln\left(C_A + \frac{\eta}{2}\right) + \left(C_A - \frac{\eta}{2}\right)\ln\left(C_A - \frac{\eta}{2}\right) + \\ + \left(C_B - \frac{\eta}{2}\right)\ln\left(C_B - \frac{\eta}{2}\right) + \left(C_B + \frac{\eta}{2}\right)\ln\left(C_B + \frac{\eta}{2}\right)\end{array}\right), \end{aligned} \tag{15}$$

$$\begin{aligned} g^{L1_2} &= 6\left(C_A V_{AA} + C_B V_{BB}\right) + 12 C_A C_B V_{mix} + \frac{3}{4}V_{mix}\eta^2 + \\ &+ \frac{kT}{4}\left(\begin{array}{l}\left(C_A - 3\frac{\eta}{4}\right)\ln\left(C_A - 3\frac{\eta}{4}\right) + \left(C_B + 3\frac{\eta}{4}\right)\ln\left(C_B + 3\frac{\eta}{4}\right) + \\ + 3\left(C_B - \frac{\eta}{4}\right)\ln\left(C_B - \frac{\eta}{4}\right) + 3\left(C_A + \frac{\eta}{4}\right)\ln\left(C_A + \frac{\eta}{4}\right)\end{array}\right). \end{aligned} \tag{16}$$

If we now simulate, using SKMF method, the interdiffusion in the diffusion couple A–B, both materials with f.c.c. lattice and with coherent initial interface between them, and take the following interaction energies: $V_{AA} = -1\cdot10^{-21}$ J, $V_{BB} = -1\cdot10^{-21}$ J, $V_{BB} = -14.04\cdot10^{-21}$ J only within the first coordination shell, we get the following typical concentration profile and typical 'occupation probabilities map' (Fig. 1).

One may see that the profile in Fig. 1 is very far from the typical experimental concentration profiles after reactive diffusion with almost horizontal concentration plateau corresponding to intermediate compounds with almost stoichiometric composition and with distinct concentration steps between these plateaus. Similar problems are encountered also in case of Monte Carlo simulation of reactive diffusion with formation of the ordered intermediate phases [26, 27].

To avoid this problem, we use the model accounting interaction within two coordination shells. In mean-field approximation, the Gibbs free energy for the disordered solution and for intermediate ordered phases acquires the following form:

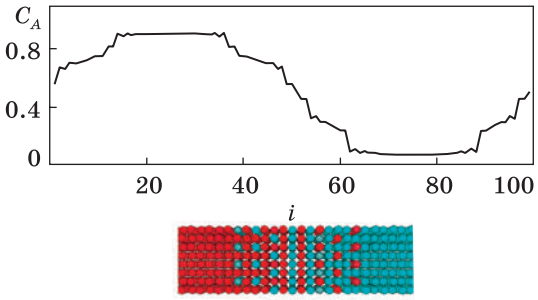

Fig. 1. Snapshots of the concentration profile (averaged over each couple of (100) planes), and the corresponding occupation probabilities map at some moment of interdiffusion in the couple *A*–*B*. Profile contains three subregions corresponding to three ordered intermediate phases but does not contain (at least, in visible form), the concentration steps between concentration plateau corresponding to three intermediate phases

$$g^{disordered} = 6\left(C_A V_{AA}^I + C_B V_{BB}^I\right) + 3\left(C_A V_{AA}^{II} + C_B V_{BB}^{II}\right) + \\ + 12 C_A C_B \left(V_{mix}^I + \frac{1}{2} V_{mix}^{II}\right) + kT\left(C_A \ln C_A + C_B \ln C_B\right), \tag{17}$$

$$g^{L1_0} = 6\left(C_A \cdot V_{AA}^I + C_B \cdot V_{BB}^I\right) + 3\left(C_A \cdot V_{AA}^{II} + C_B \cdot V_{BB}^{II}\right) + \\ + 12 C_A C_B \cdot V_{mix}^I + 6 C_A C_B \cdot V_{mix}^{II} + \left(V_{mix}^I - \frac{3}{2} V_{mix}^{II}\right)\eta^2 + \\ + \frac{kT}{2}\left(\begin{array}{l}\left(C_A + \frac{\eta}{2}\right)\ln\left(C_A + \frac{\eta}{2}\right) + \left(C_A - \frac{\eta}{2}\right)\ln\left(C_A - \frac{\eta}{2}\right) \\ + \left(C_B - \frac{\eta}{2}\right)\ln\left(C_B - \frac{\eta}{2}\right) + \left(C_B + \frac{\eta}{2}\right)\ln\left(C_B + \frac{\eta}{2}\right)\end{array}\right), \tag{18}$$

$$g^{L1_2} = 6\left(C_A \cdot V_{AA}^I + C_B \cdot V_{BB}^I\right) + 3\left(C_A \cdot V_{AA}^{II} + C_B \cdot V_{BB}^{II}\right) + \\ + 12 C_A C_B \cdot V_{mix}^I + 6 C_A C_B \cdot V_{mix}^{II} + \frac{3}{4}\left(V_{mix}^I - \frac{3}{2} V_{mix}^{II}\right)\eta^2 + \\ + \frac{kT}{4}\left(\begin{array}{l}\left(C_A - 3\frac{\eta}{4}\right)\ln\left(C_A - 3\frac{\eta}{4}\right) + \left(C_B + 3\frac{\eta}{4}\right)\ln\left(C_B + 3\frac{\eta}{4}\right) \\ + 3\left(C_B - \frac{\eta}{4}\right)\ln\left(C_B - \frac{\eta}{4}\right) + 3\left(C_A + \frac{\eta}{4}\right)\ln\left(C_A + \frac{\eta}{4}\right)\end{array}\right). \tag{19}$$

To obtain the reasonable phase diagram with intermediate compounds with narrow concentration ranges and distinct concentration intervals between these ranges, we choose the mixing energy in the first coordination shell as negative (which is standard choice) and the mixing energy in the second coordination shell as positive. Moreover, we choose their magnitudes in such a way, that

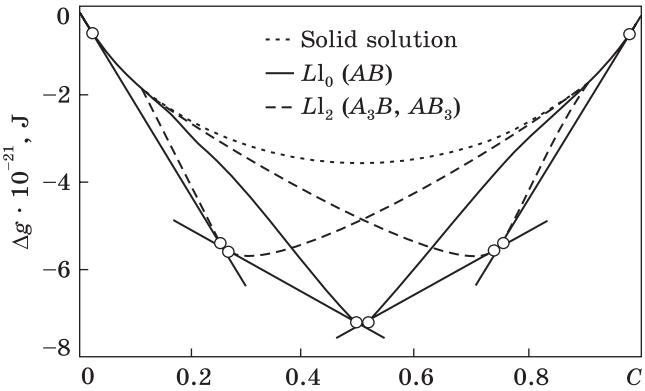

Fig. 2. Composition dependences of the Gibbs free energy per atom, $\Delta g(C)$, for disordered phase and ordered phases A_3B, AB and AB_3 at T=750 K, constructed in the frame of mean-field approximation

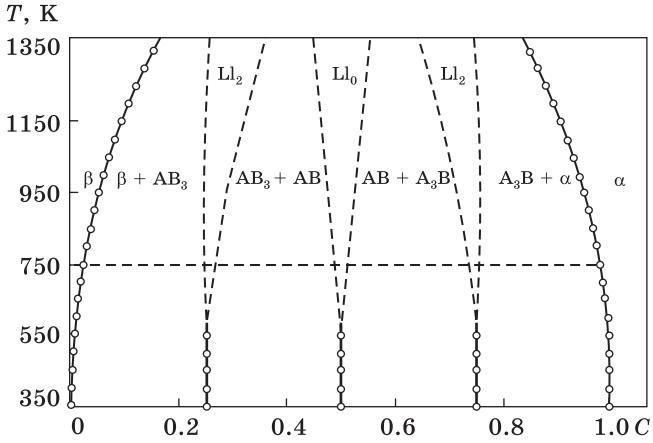

Fig. 3. Dependences T–C for the margins of the concentration ranges of all existing phases in A–B system calculated by the common tangents' rule

(1) the effective mixing energy for the disordered phases, $\left(V^I_{mix} + \frac{1}{2}V^{II}_{mix}\right)$ is positive (so that disordered phase has a tendency to decomposition), and

(2) the energy for the ordered phases (coefficient before the squared order parameter), $\left(V^I_{mix} - \frac{3}{2}V^{II}_{mix}\right)$, is negative.

For example, let us take the following interaction energies: $V^I_{AA} = V^I_{BB} = -10^{-21}$ J, $V^I_{AB} = -3.9 \cdot 10^{-21}$ J, $V^{II}_{AA} = V^{II}_{BB} = -8.76 \cdot 10^{-21}$ J, $V^{II}_{AB} = -2 \cdot 10^{-21}$ J.

Then, we construct the curve $\Delta g(T,C) = g(T,C) - C \cdot g(T,C = 1) - (1 - C) \cdot g(T,C = 0)$ for disordered phase directly according to eq. (17). In Eqs. (18), (19), we at first minimize $\Delta g(T, C, \eta)$ in respect to η at any concentration C and temperature T. It gives the following curves $\Delta g(C)$ for disordered phase and ordered phases A_3B, AB and AB_3 at T = 750 K (see Fig. 2).

Building such curves at various temperatures, and using the common tangent construction, we obtained the phase diagram [22] of our

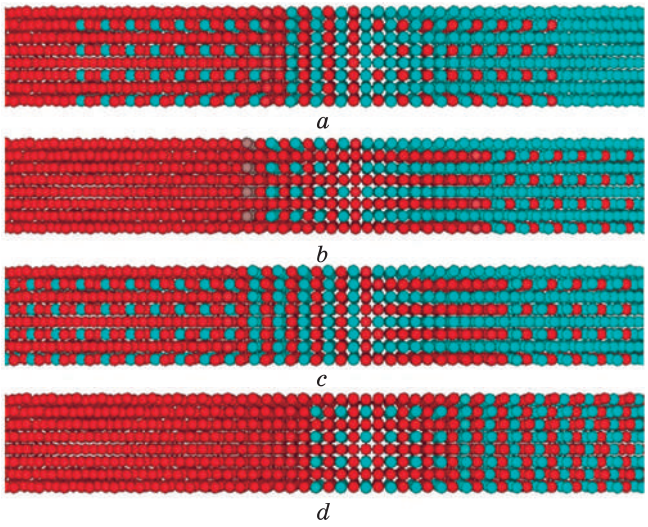

Fig. 4. Possible incremental diffusion couples: (*a*) *A*–*B* with three growing ordered phases A_3B ($L1_2$), *AB* ($L1_0$) and AB_3 ($L1_2$) (*b*) *A*–AB_3 with two growing ordered phases A_3B and *AB*, (*c*) A_3B–AB_3 with single growing ordered phase *AB*, (*d*) *A*–*AB* with single growing phase A_3B

model system, and at once checked it by the method of diffusion couples. For example, we constructed the thin-film diffusion couple *A*–ordered A_3B, and simulated interdiffusion until full equilibrium — two plateaus with concentrations corresponding to two ends of the same tie line between solution of *B* in *A* and compound A_3B (see Fig. 3).

After this we simulated interdiffusion in the diffusion couples with various starting compositions (incremental diffusion couples) — Fig. 4.

Now we show some of simulation results. Concentration is averaged over each couple of (100)-planes.

Simulation of diffusion in *A*–*AB* couple (Fig. 5) shows the formation of A_3B concentration plateau with distinct concentration steps between this phase and parent phases *A* and *AB*. Width of this plateau (actually, of its ratio to the total size of diffusion couple) grows parabolically. The rate constants obey Arrhenius law.

It is interesting to compare the simulation results with analytical predictions, obtained in the frame of Matano–Boltzmann–Wagner analysis. It is well known that the kinetics of phase layer growth is determined by Wagner diffusivity, which is the integral of interdiffusivity over the concentration range of intermediate phase [28, 29]. In the frame of Matano–Boltzmann analysis for the infinite diffusion couple with terminal concentrations C_L, C_R,

$$\tilde{D}(C) = -\frac{1}{2t\left.\dfrac{dc}{dx}\right|_C} \int_{C_L}^{C} (x - x_M)\, dc\,, \tag{20}$$

and we derived the following expression for Wagner diffusivity, and used it for direct calculation of Wagner diffusivity (here, x_M is a Ma-

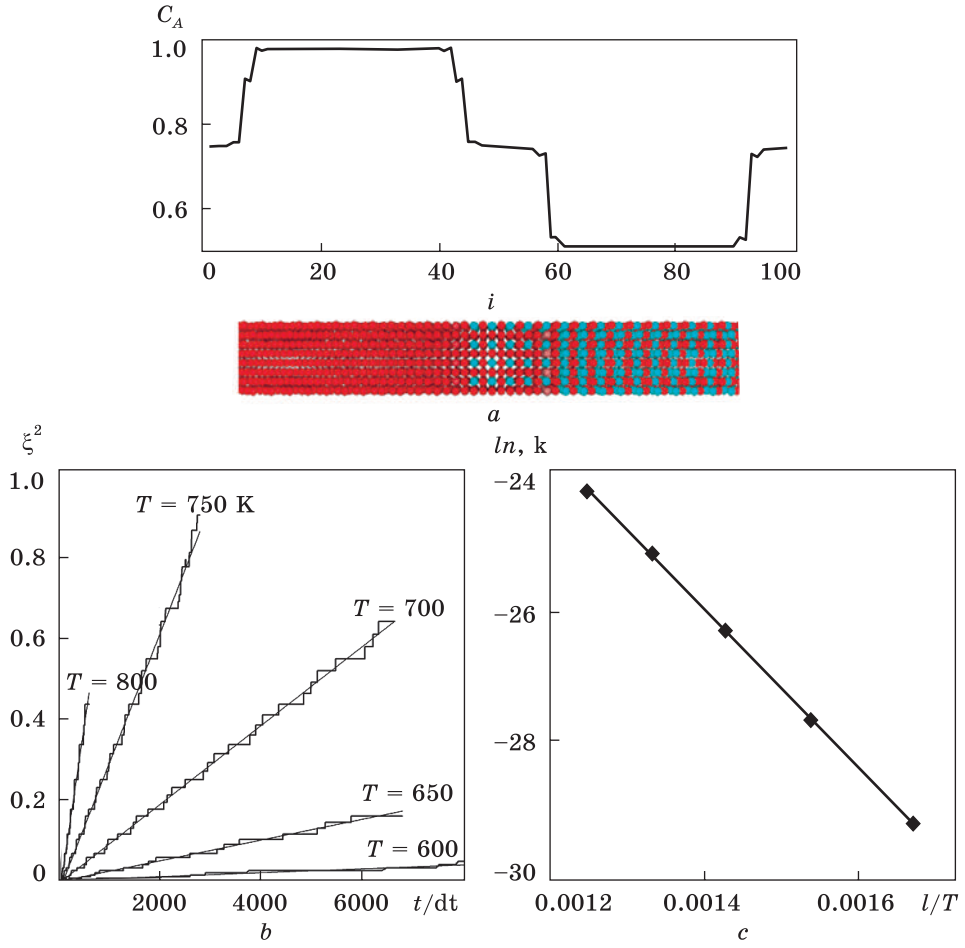

Fig. 5. (*a*) Concentration profile (averaged over each couple of neighbouring (100) planes and site occupation map, (*b*) time dependence of the squared reduced phase width $\xi = 2\Delta x/L$ (L is a total width of the diffusion couple), (*c*) Arrhenius-type dependence of growth rate constants on inverse temperature

tano plane coordinate):

$$D_W \equiv \int_{C_L}^{C_R} \tilde{D}(C)\, dC = \frac{1}{2t} \int_{x_L}^{x_R} dx \int_{C_L}^{C(x)} \left(x_M - x(c')\right) dc' \tag{21}$$

or, in discreet form,

$$D_W = \frac{(dx)^2}{2t} \sum_{i=iL}^{iR-1} \sum_{j=iL}^{i+1} (iM - j)\,(C[j+1] - C[j])\,. \tag{22}$$

Here, $dx = x[i+1] - x[i]$, $iM \equiv \sum_{i=iL}^{iR-1} i \cdot (C[i+1] - C[i]) \Big/ (C_R - C_L)$.

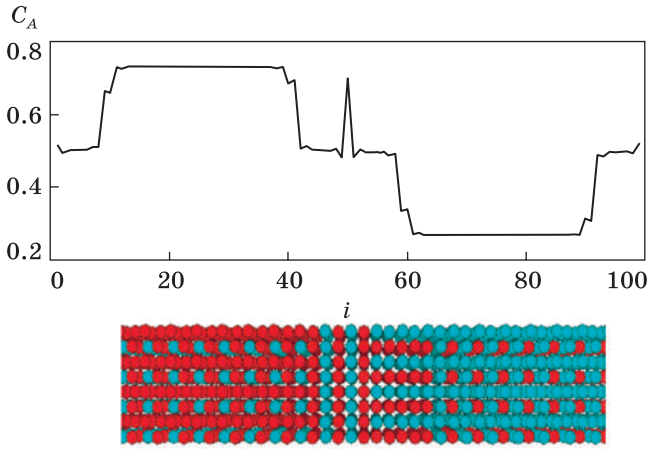

Fig. 6. Growth of single intermediate phase AB in the couple A_3B–AB_3: Concentration profile (averaged over each couple of neighbouring (100) planes, and the site occupation map

If one adopts the steady-state approximation (almost the same flux at both boundaries of the same phase layer), which works very well for growing phase layers with narrow concentration range [30], if one also neglects the solubility of B in A-solution and treats intermediate phase A_3B as almost stoichiometric, then the flux balance equations for the growth of this phase boundaries (left L and right R) in the couple A–A_3B have the following simple form:

$$\begin{cases} \left(\frac{1}{4}-0\right)\frac{dx_L}{dt} = -\frac{\tilde{D}\Delta C}{\Delta x} \Rightarrow \frac{dx_L}{dt} = -4\frac{\tilde{D}\Delta C}{\Delta x} \\ \left(\frac{1}{2}-\frac{1}{4}\right)\frac{dx_R}{dt} = +\frac{\tilde{D}\Delta C}{\Delta x} \Rightarrow \frac{dx_R}{dt} = +4\frac{\tilde{D}\Delta C}{\Delta x} \end{cases} \Rightarrow \Delta x^2 = 16\left(\tilde{D}\Delta C\right)^{A_3B} t\,, \quad (23)$$

or, for reduced phase thickness,

$$\xi^2 = k_1^{A_3B}\frac{t}{dt} = 4\left(\frac{\Delta x}{L}\right)^2 = \frac{64dt}{L^2}\left(\tilde{D}\Delta C\right)^{A_3B}\frac{t}{dt}\,, \quad (24)$$

$$\left(\tilde{D}\Delta C\right)^{A_3B} = k_1^{A_3B}\frac{L^2}{64dt}\,, \quad (25)$$

$$\frac{\left(N_x\right)^2 dX^2}{64dt}k = 7.8\cdot 10^{-14}\ \text{m}^2/\text{s}\,.$$

On the other hand, direct calculation of Wagner coefficient according to eq. (22) via direct Matano–Boltzmann calculation gives $7.0\cdot 10^{-14}$ m^2/s. We can see that the difference seems reasonable — within 10 percent.

Analogical results are obtained for the growth of single ordered phase AB in the couple A_3B–AB_3 (see Fig. 6).

Note that the growing phase layer, in our case, consists of two sublayers representing two antiphase domains of the AB ordering, with

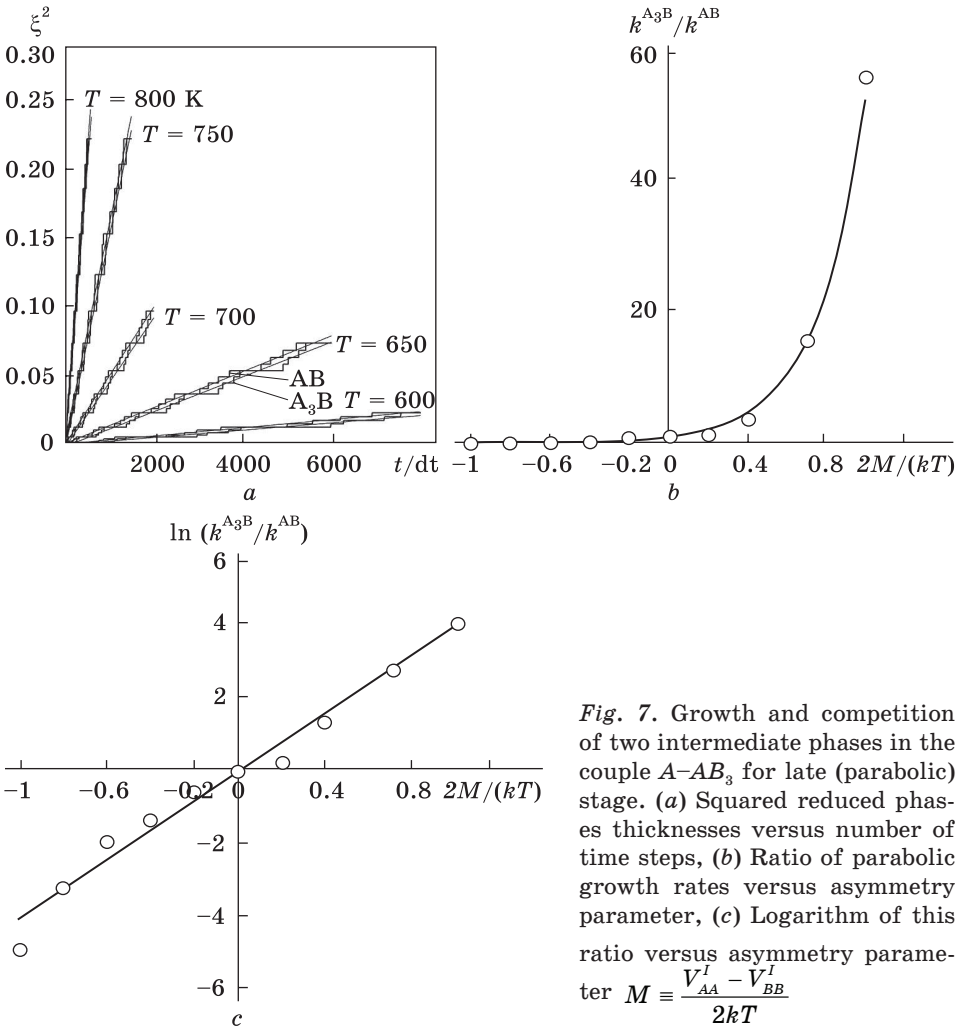

Fig. 7. Growth and competition of two intermediate phases in the couple A–AB_3 for late (parabolic) stage. (*a*) Squared reduced phases thicknesses versus number of time steps, (*b*) Ratio of parabolic growth rates versus asymmetry parameter, (*c*) Logarithm of this ratio versus asymmetry parameter $M \equiv \frac{V_{AA}^I - V_{BB}^I}{2kT}$

different orientations of AB-'zebra'. Boundary between two domains (sublayers) corresponds to a peak in the middle of concentration plateau.

Analytic solution in the steady-state approximation and under assumption of practically stoichiometric compounds A_3B, AB and AB_3 gives:

$$\begin{cases} \left(\frac{1}{2}-\frac{1}{4}\right)\frac{dx_L}{dt} = -\frac{\tilde{D}_{AB}\Delta c}{\Delta x} \\ \left(\frac{3}{4}-\frac{1}{2}\right)\frac{dx_R}{dt} = +\frac{\tilde{D}\Delta c}{\Delta x} \end{cases} \Rightarrow \Delta x^2 = 16\left(\tilde{D}_{AB}\Delta C\right)^{AB} t\,. \qquad (26)$$

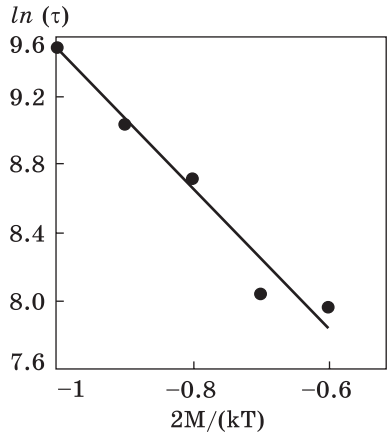

Fig. 8. Suppression of A_3B-phase at the initial stage: logarithm of delay time versus reduced asymmetry parameter

So, $\left(\tilde{D}\Delta C\right)^{AB} = k_1^{AB}\dfrac{L^2}{64dt} = 7.4\cdot 10^{-14}$ m^2/s, and direct Matano–Boltzmann calculation according to eq. (22) gives $\overline{\tilde{D}\Delta C} = 7.8\cdot 10^{-14}$ m^2/s.

Thus, the difference between the values of Wagner diffusivity, obtained via (1) analytic solution from the parabolic time dependence of the phase plateau thickness, and, alternatively, (2) via direct Matano–Boltzmann calculation, is even less than in previous couple (within 5 percent).

Even more interesting are the results for the competition of two intermediate phases, obtained from simulation of the couple A–AB_3 (see Fig. 7). At the late stage, both phases grow parabolically, and the ratio of rate constants exponentially depends on the diffusion asymmetry parameter $\dfrac{V_{AA}^I - V_{BB}^I}{kT}$, which is directly related to the difference of interatomic interaction energies between two materials:

$$k^{A_3B} / k^{AB} \approx \exp(8M) = \exp\left(4\frac{V_{AA}^I - V_{BB}^I}{kT}\right). \qquad (27)$$

At the initial stage of phase competition and under significant diffusion asymmetry, the formation of one of two phases is temporarily suppressed, and the time delay (incubation time) also exponentially depends on the diffusion asymmetry (see Fig. 8):

$$\tau^{delay} \approx \text{const}\cdot\exp\left(4\frac{V_{AA}^I - V_{BB}^I}{kT}\right)$$

3. Monte Carlo Simulation of Reactive Diffusion

Similar trick with two coordination shells with opposite signs of mixing energy we tried in Monte Carlo simulations [31]. Results are similar, but, of course, due to Monte Carlo peculiarities, the concentration curves are not so smooth anymoreю.

Just for illustration, we show the typical concentration profile (averaged over *YZ*-planes) and snapshot of components redistribution during Monte Carlo simulation of A–AB_3 diffusion couple (Fig. 9). We can see the distinct plateau for both phases and sharp interfaces between them.

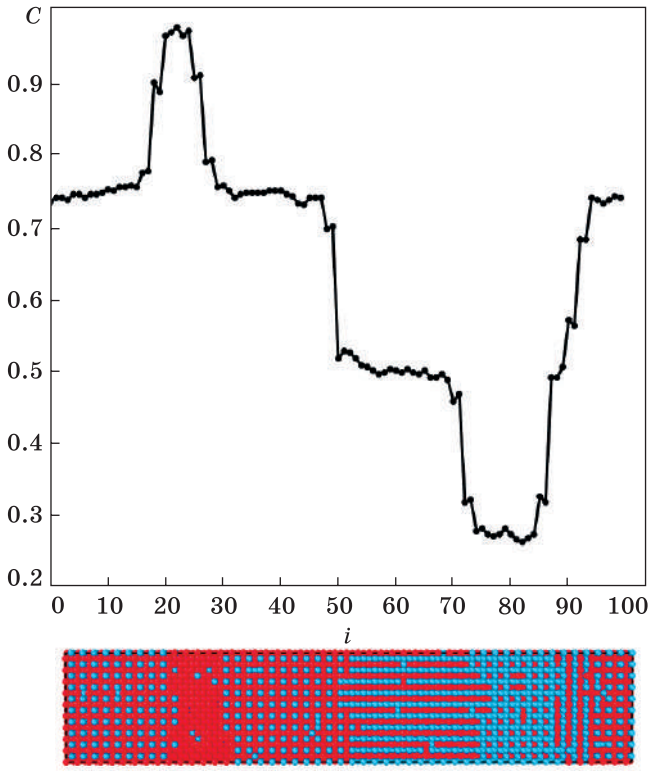

Fig. 9. Typical concentration profile (averaged over each pair of neighbouring *YZ*-planes) and snapshot of components redistribution during Monte Carlo simulation of A–AB_3 diffusion couple. Parameters $V^{I}_{mix} = -2.9 \times 10^{-21}$ J, $V^{II}_{mix} = +6.76 \times 10^{-21}$ J, $T = 750$ K

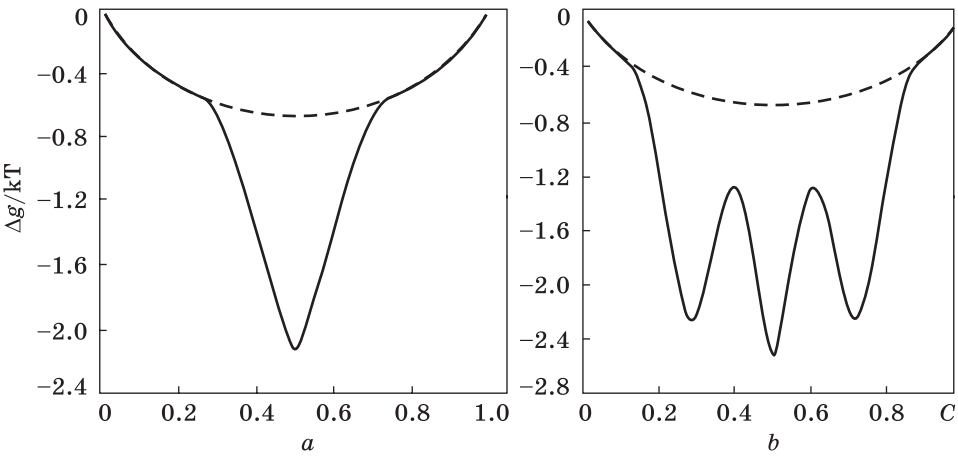

Fig. 10. Account of interactions depending on local surrounding, in Gibbs free energy per atom for the case of single (*a*) and three (*b*) intermediate compounds

We also try alternative way to get steep plateau and distinct interfaces in simulation. The main idea is an account of interactions depending on local surrounding of interacting atoms. We suggest the exponen-

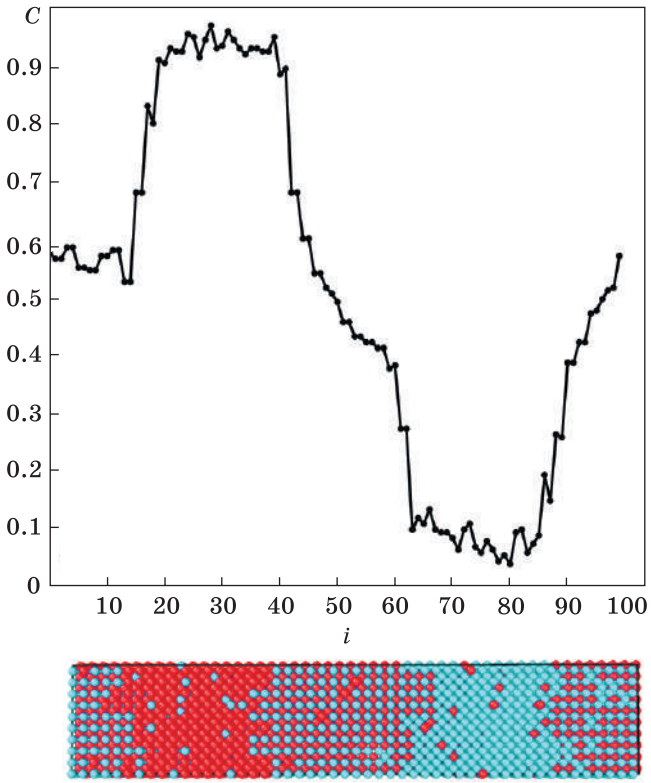

Fig. 11. Concentration profile (averaged over each couple of atomic *YZ* planes) and corresponding snapshot of the cross-section, obtained by MC-simulation of b.c.c.-couple *A*–*B* with composition-dependent interactions

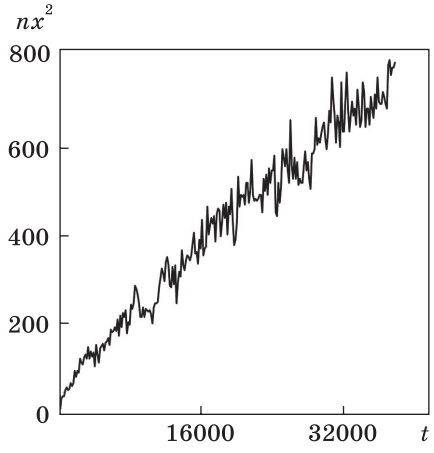

Fig. 12. Squared number of planes with average concentration within the range (0.425–0.575 versus number of Monte Carlo steps). $E_R = 8.5$

tial dependency of interaction intensity on the squared deviation of cluster concentration from the stoichiometric value, corresponding to the strongest bond energy [32]:

$$\frac{V_{mix}}{k_B T} = -\frac{E_R}{Z} \exp\left(-\alpha \left(C_{cluster} - C_{IMC}\right)^2\right), \tag{29}$$

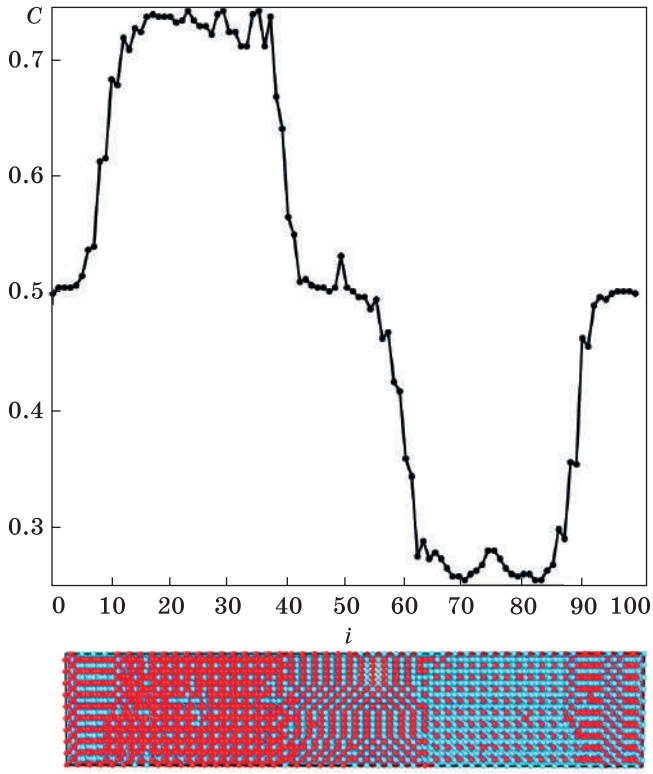

Fig. 13. Concentration profile (local concentrations averaged over planes *YZ*) and snapshot of cross-section for the transient moment of interdiffusion in A_3B–AB_3 couple

$$E_R = \frac{Z\left|E_{mix}\right|}{k_B T},$$

$$\frac{V_{mix}}{k_B T} = -\frac{E_{R1}}{Z}\exp\left(-\alpha_1 (C_{cluster} - 1/4)^2\right) - \frac{E_{R2}}{Z}\exp\left(-\alpha_2 (C_{cluster} - 1/2)^2\right) - \frac{E_{R3}}{Z}\exp\left(-\alpha_3 (C_{cluster} - 3/4)^2\right). \quad (30)$$

In Fig. 10, we show the characteristic Gibbs free energy dependence on concentration for the cases of single intermediate phase and three intermediate phases with nonlinear concentration dependence of interatomic interactions.

Cluster concentration around interacting atoms is calculated as follows: at first, we calculate an average concentration within both subclusters around each atom, and then we take the average:

$$C_{cluster} = \frac{\bar{C}(i) + \bar{C}(j)}{2}. \quad (31)$$

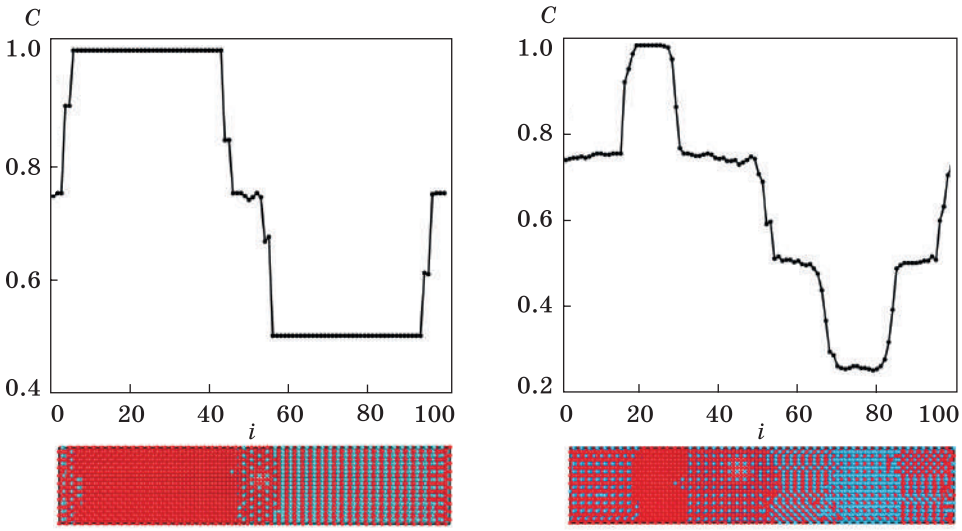

Fig. 14. Couple A–AB. Single ordered intermediate phase A_3B with structure $L1_2$ is formed and grows

Fig. 15. Couple A–AB_3. Two ordered intermediate phases A_3B with structure $L1_2$ and AB with structure $L1_0$ are formed and grow simultaneously

In case of b.c.c. lattice,

$$\overline{C}(i) = \frac{C(i) + \frac{1}{8}\sum_{in}^{8} C(i)}{2}, \tag{32a}$$

$$\overline{C}(j) = \frac{C(j) + \frac{1}{8}\sum_{jn}^{8} C(j)}{2}. \tag{32b}$$

In case of f.c.c. lattice,

$$\overline{C}(i) = \frac{C(i) + \frac{1}{4}\sum_{in=1}^{12} C(in)}{4}, \tag{33a}$$

$$\overline{C}(j) = \frac{C(j) + \frac{1}{4}\sum_{jn=1}^{12} C(jn)}{4}. \tag{33b}$$

Here, we show the results of simulation of the intermediate AB-layer growth (with structure B_2) in b.c.c. diffusion couple. Interfaces are not as distinct as in previous cases, but quite sufficient to distinguish the different phases (see Fig. 11).

Parabolic law for the square phase thickness is also satisfied (more or less) (see Fig. 12).

Another example is a simulation of interdiffusion in f.c.c. lattice between ordered A_3B and ordered AB_3 phases, when the ordered phase AB ($L1_0$) is growing in the contact zone (Fig. 13).

Similar picture is obtained in Monte Carlo simulation of the f.c.c. couple A–AB. Single ordered intermediate phase A_3B with structure $L1_2$ is formed and grows (Fig. 14).

We also made Monte Carlo simulation of the couple A–AB_3. Two ordered intermediate phases A_3B with structure $L1_2$ and AB with structure $L1_0$ are formed and grow simultaneously (Fig. 15).

4. New Phenomenological Results in Description of Reactive Diffusion

4.1. Generalization of the Wagner Diffusivity Concept

Now, we come to some new phenomenological results in reactive diffusion description. First of these results is related to the generalization of Wagner diffusivity concept, which was introduced as an integral of interdiffusion coefficient over the concentration range of some phase:

$$D_W\left(\text{phase } k\right) = \int\limits_{\Delta N(k)} \tilde{D}\left(N\right) dN\,. \tag{34}$$

Wagner diffusivity is a very useful concept for description of reactive phase growth with very narrow concentration range. Sometimes, one can even say that this concentration range tends to zero. In this case, the thermodynamic factor of the interdiffusion coefficient tends to infinity, so that the product of average (over the concentration range) interdiffusion coefficient and concentration interval remains finite and reasonable. Indeed, according to the common tangent rule, applied to equilibria of intermediate compound with the 'right' and 'left' phases, tending of concentration interval between 'right' and 'left' points of contact tangents is proportional to the second derivative of Gibbs free energy pet atom over concentration. Thus, when $\Delta C_B \to 0$, then,

$$\tilde{\bar{D}} = < (C_A D_B^* + C_B D_A^*) \frac{C_A C_B}{k_B T} \frac{\partial^2 g}{\partial C_B^2} > \to \infty\,, \tag{35}$$

$\tilde{D}\Delta C_B \to \infty \times 0 = D_W \neq 0\, and \neq \infty$.

Let us explain this point more rigorously and explicitly. Wagner diffusivity can be expressed in terms of combination of the tracer diffusivities of both components multiplied by the thermodynamic driving force of the phase formation from the neighbouring phases [8]. Indeed, if one substitutes Darken expression for interdiffusion coefficient into the integral (24), one gets:

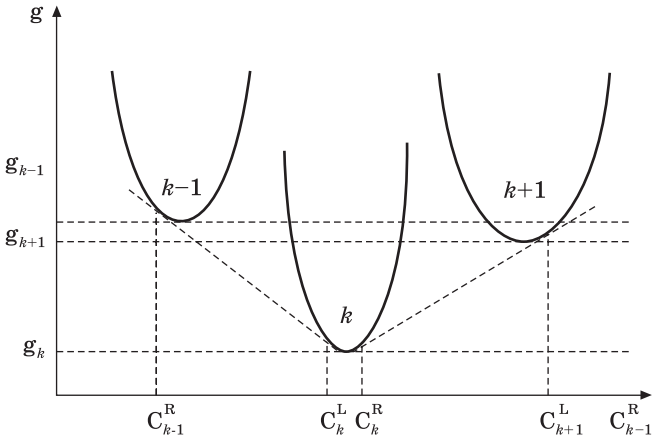

Fig. 16. Schematic picture of common tangents rule and thermodynamic driving force for narrow intermediate phases, used for derivation of explicit form (36) of the Wagner diffusivity

$$D_W\left(\text{phase } k\right) = \int\limits_{\Delta C_k=\left(C_k^L, C_k^R\right)} \tilde{D}\left(C_B\right) dC_B =$$

$$= \int\limits_{C_k^L}^{C_k^R} \left((1-C)D_B^* + CD_A^*\right) \frac{(1-C)\,C}{k_B T} \frac{\partial^2 g}{\partial C^2}\, dC =$$

$$= \overline{\left((1-C)D_B^* + CD_A^*\right) \frac{(1-C)\,C}{k_B T}} \int\limits_{C_k^L}^{C_k^R} \frac{\partial^2 g}{\partial C^2}\, dC \approx$$

$$\approx \left((1-C_k)\overline{D_B^*(k)} + C_k \overline{D_A^*(k)}\right) \frac{(1-C_k)\,C_k}{k_B T} \left(\left(\frac{\partial g}{\partial C}\right)^{common}_{k/k+1} - \left(\frac{\partial g}{\partial C}\right)^{common}_{k-1/k} \right) =$$

$$\approx \left((1-C_k)\overline{D_B^*(k)} + C_k \overline{D_A^*(k)}\right) \frac{(1-C_k)\,C_k}{k_B T} \left(\frac{g_{k+1}-g_k}{C_{k+1}-C_k} - \frac{g_k - g_{k-1}}{C_k - C_{k-1}} \right).$$

Here, we used, first, the theorem $\int\limits_a^b f(x)\,\varphi(x)\,dx = \overline{f} \cdot \int\limits_a^b \varphi(x)\,dx$, where 'mean value' $\overline{f}$ is a value of function f with some 'mean' (more accurately, intermediate) argument $\overline{f} = f(\overline{x})$, $a < \overline{x} < b$. Secondly, we used the fact of narrow concentration range, so that the "mean" (in general, unknown) intermediate value within concentration range is, anyway, close to the stoichiometric value C_k, Also, in the common tangent equations (see Fig. 16) $\left(\left(\frac{\partial g}{\partial C}\right)^{common}_{k/k+1} \approx \frac{g_{k+1}-g_k}{C_{k+1}-C_k}, \left(\frac{\partial g}{\partial C}\right)^{common}_{k-1/k} \approx \frac{g_k - g_{k-1}}{C_k - C_{k-1}} \right)$, we approximated the values of $g(C)$ in the points of contact tangent by the minimal value of this function $g(C_k^L) \approx g(C_k^R) \approx \min g(C, C_k^L < C < C_k^L) \equiv g_k$.

On the other hand, the thermodynamic driving force of reaction phase$(k-1)$ + phase$(k+1)$ → phase(k) can be found as

$$\Delta g\left(k-1,k+1\to k\right)=\left(\frac{C_k-C_{k-1}}{C_{k+1}-C_{k-1}}g_{k+1}+\frac{C_{k+1}-C_k}{C_{k+1}-C_{k-1}}g_{k-1}\right)-g_k,$$

and difference of 'right' and 'left' first derivatives for the right and left common tangents is:

$$\frac{g_{k+1}-g_k}{C_{k+1}-C_k}-\frac{g_k-g_{k-1}}{C_k-C_{k-1}}=$$
$$=\frac{(C_k-C_{k-1})g_{k+1}-(C_k-C_{k-1})g_k-(C_{k+1}-C_k)g_k+(C_{k+1}-C_k)g_{k-1}}{(C_{k+1}-C_k)(C_k-C_{k-1})}=$$
$$=\frac{(C_{k+1}-C_{k-1})}{(C_{k+1}-C_k)(C_k-C_{k-1})}\frac{(C_k-C_{k-1})g_{k+1}+(C_{k+1}-C_k)g_{k-1}-(C_{k+1}-C_{k-1})g_k}{(C_{k+1}-C_{k-1})}=$$
$$=\frac{(C_{k+1}-C_{k-1})}{(C_{k+1}-C_k)(C_k-C_{k-1})}\Delta g\,(k-1,k+1\to k).$$

Thus,

$$D_W(\text{phase }k)=((1-C_k)\overline{D_B^*(k)}+C_k\overline{D_A^*(k)})\times$$
$$\times\frac{(1-C_k)\,C_k\,(C_{k+1}-C_{k-1})}{(C_{k+1}-C_k)(C_k-C_{k-1})}\frac{\Delta g\,(k-1,k+1\to k)}{k_BT}. \qquad (36)$$

Thus, Wagner diffusivity is proportional to the product of mean mobility (actually, combination of mean tracer diffusivities) and to the driving force of this phase production.

In the case of single intermediate phase growth, the time law for the squared phase layer thickness is described as well by Wagner diffusivity multiplied by time — this equation is very well known [8]:

$$\frac{d\Delta X}{dt}=\frac{D_W}{C_{IMC}(1-C_{IMC})}\frac{1}{\Delta X}\Rightarrow(\Delta X)^2=\frac{2D_W}{C_{IMC}(1-C_{IMC})}t. \qquad (37a,b)$$

It is less known that we can express the average squared interpenetration distance also in terms of Wagner interdiffusivity [29].

$$<(X-X_M)^2>\equiv\frac{\int_{C_L}^{C_R}(X-X_M)^2dC}{C_R-C_L}=\frac{2D_W(C_L,C_R)}{C_R-C_L}\cdot t. \qquad (38)$$

Let us prove it. We start from Boltzmann–Matano transformation of the second Fick's law under initial and boundary conditions compatible with parabolic substitution $C(t,x)=C(\xi=(X-X_M)/\sqrt{t})$:

$$-\frac{1}{2}\xi\frac{dC}{d\xi}=\frac{d}{d\xi}\left(\tilde{D}(C)\frac{dC}{d\xi}\right).$$

This equation can be found in any book on mathematics of diffusion. All we need to do now is to multiply both parts of this equation by x and integrate over total length of diffusion couple (formally, from minus infinity to plus infinity). Then,

$$-\frac{1}{2}\int_{-\infty}^{\infty}\xi^2\frac{dC}{d\xi}d\xi=\int_{-\infty}^{\infty}\xi\frac{d}{d\xi}\left(\tilde{D}(C)\frac{dC}{d\xi}\right)d\xi. \tag{39}$$

Elementary transformations of the left-hand side and right-hand side of eq. (39) give:

$$\begin{aligned}-\frac{1}{2}\int_{C_L}^{C_R}\xi^2 dC&=\xi\cdot\tilde{D}(C)\frac{dC}{d\xi}\Big|_{-\infty}^{\infty}-\int_{-\infty}^{\infty}\left(\tilde{D}(C)\frac{dC}{d\xi}\right)d\xi=\\&=0-\int_{N_L}^{N_R}\tilde{D}(C)dC=-D_W(C_L,C_R).\end{aligned} \tag{40}$$

Eq. (40) immediately leads to eq. (38). So, the theorem is proved.

If system contains several intermediate phases and marginal solid solutions, one should just take the function $\tilde{D}(N)$ equal to zero within all two-phase intervals, since within any two-phase interval of binary system the gradient of concentration means zero gradient of chemical potentials and, hence, zero flux, which is equivalent to zero interdiffusivity. Then, eq. (38) transforms into

$$<(\Delta X)^2>=2\left(\int_0^{C_\alpha}\tilde{D}(C)\,dC+\sum_{k=1}^{n}\int_{(\Delta C_k)}\tilde{D}_k(C)\,dC+\int_{C_\beta}^{1}\tilde{D}(C)\,dC\right)t. \tag{41}$$

To the best of our knowledge, nobody before us [29] obtained the generalization of the property (37) on the case of average squared interpenetration distance for arbitrary number of intermediate phases. Actually, it is a kind of superposition law for Wagner diffusivity. Once more: average squared interpenetration distance is equal to the product 2 multiplied by time and multiplied by the sum of Wagner diffusivities for all intermediate phases and also of terminal solid solutions.

4.2. Synergy of Phase Layer Growth and Lateral Grain Growth during Reactive Diffusion at Low Temperatures

Another fresh semi-phenomenological result is an idea of a so-called Flux-Driven Lateral Grain Growth. Lateral grain growth accompanies intermetallic compound growth. Moreover, it can be induced by reactive phase transformation at low temperatures (at frozen bulk diffusion). In its turn, the evolution of grain size influences the rate of diffusive reaction. This synergy of the Reaction-Driven Grain Growth and Diffusion-controlled Reaction was recently analysed [33]. Power laws for the intermetallic compound growth with time exponent 0.4 and the lateral grain growth

with time exponent 0.2 were predicted. Let us see the details.

In general, one should distinguish two different mechanisms of lateral Grain growth during reactive growth of the phase layer with longitudinal bamboo structure.

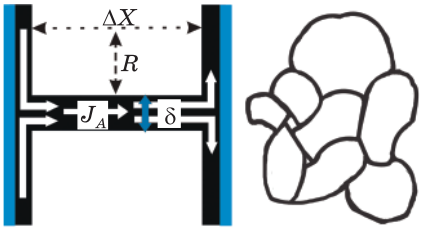

a *b*

Fig. 17. Diffusion-controlled phase growth by diffusion along GB in the bamboo structure. Longitudinal (*a*) and lateral (*b*) cross-sections.

First mechanism (Fig. 17) is an ordinary curvature-driven lateral grain growth simultaneously (but independently on) the phase growth. In this case, the lateral grain growth proceeds simultaneously along each entire grain-boundary and changes the mean lateral size everywhere along the thickness of phase layer. Of course, this growth decreases the effective diffusivity $\delta_{GB} D_{GB}^{CuZn} / R$, and hence, influences the rate of phase growth, but not vice versa, (phase growth does not influence the grain growth).

For simplicity, assume that the lateral size of each grain is the same along the phase layer and changes with time simultaneously in the same way in all sections. In other words, R depends on time but does not depend on coordinate within phase. Then the ratio between the fast diffusion path along the cross-section of the grain boundaries and the full cross-section of the grain is $\left(\frac{1}{2}\delta \cdot 2\pi R\right) / \pi R^2 = \delta / R$, so that the effective diffusivity across the layer is

$$D^{effective}(t) \approx \frac{\delta}{R(t)} D_{GB}^{i}. \tag{42}$$

Substitution of eq. (42) into eq. (37a) gives:

$$\frac{d\Delta X^i}{dt} \approx \frac{\delta D_{GB}^{i}}{C^i(1-C^i)} \frac{1}{R} \frac{\Delta C^i}{\Delta X^i}. \tag{43}$$

Now we consider the typical case when the diameter $2R$ of the bamboo-type grain in the IMC grows with time according to power law $R = At^m$, $m < 1$. Then,

$$(\Delta X)^1 d\Delta X \approx 4\delta_{GB} D_{GB}^{\mathrm{CuZn}} (C_{\mathrm{Zn}}^{\beta/\mathrm{Sn}} - C_{\mathrm{Zn}}^{\beta-\mathrm{inter}}) \frac{dt}{At^m}, \tag{44}$$

$$\Delta X = \left(\frac{8}{1-m} \mathrm{d}_{GB} D_{GB}^{\mathrm{CuZn}} (C_{\mathrm{Zn}}^{\mathrm{b}/\mathrm{Sn}} - C_{\mathrm{Zn}}^{\mathrm{b}-\mathrm{inter}}) / A \right)^{1/2} t^{\frac{1-m}{2}}. \tag{45}$$

For example, if the lateral grain growth obeys parabolic law ($m = 0.5$), typical for normal grain growth, then the time exponent for phase growth becomes $n = (1 - 1/2)/2 = 0.25$. Another familiar possibility is similar to Flux-Driven Ripening [34–36]: $m = 1/3$, $n = (1 - 1/3)/2 = 1/3$.

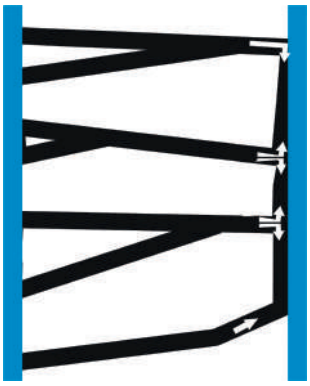

Fig. 18. Lateral grain growth induced by phase growth

Second mechanism of grain growth (Fig. 18) proceeds only at the joints of grain-boundaries and the interphase interfaces: the upcoming (*via* grain-boundary) atoms choose the host grain according to probabilities depending on curvature.

In case of the second mechanism, we assume that the IMC growth proceeds mainly due to transfer of A atoms from interface A/(GB in IMC) to the interface (GB in IMC)/B with a consequential lateral redistribution along this interface and reaction with B. Driving force of this process coincides with the driving force of reaction, which is the gradient of chemical potentials. We assume (and it could be a reasonable assumption at comparatively low temperature) that the normal curvature driven lateral movement of grain boundaries is frozen or pinned by some impurities. We assume that the only place where the capillary forces and corresponding Gibbs-Thomson potential $\frac{\gamma\Omega}{R}$ may play a crucial role, is the redistribution of the atoms arriving at the joint, between the neighbouring grains. If lateral redistribution proceeds faster than the transport through the IMC layer, we may use the Boltzmann distribution for finding the fraction of atoms going to lone of two opposite sides of the GB junction with interface. The difference between thermodynamic driving forces of reactions at the two sides of the curved junction with curvature radius r is $\frac{\gamma\Omega}{r} = \frac{\gamma\Omega}{2r} - \left(-\frac{\gamma\Omega}{2r}\right)$. Therefore, the probabilities of sticking to one of the adjacent (to the junction with curvature radius r) grains are equal to

$$p_{+} = \exp\left(\frac{\gamma\Omega}{2rkT}\right) / \left(\exp\left(\frac{\gamma\Omega}{2rkT}\right) + \exp\left(-\frac{\gamma\Omega}{2rkT}\right)\right)$$

and

$$p_{-} = \exp\left(-\frac{\gamma\Omega}{2rkT}\right) / \left(\exp\left(\frac{\gamma\Omega}{2rkT}\right) + \exp\left(-\frac{\gamma\Omega}{2rkT}\right)\right).$$

Then, the average local lateral shift of the curved grain boundary junction with interface after the formation of a new atomic layer of thickness d will be equal to

$$\Delta y = d \tanh\left(\frac{\gamma\Omega}{2rkT}\right). \tag{46}$$

For r larger than 100 nm and temperature higher than 400 K, $\frac{\gamma\Omega}{2rkT} \ll 1 \Rightarrow \tanh\left(\frac{\gamma\Omega}{rkT}\right) \approx \frac{\gamma\Omega}{2rkT}$.

The inverse mean curvature radius r is proportional to the mean grain size (see, for example, [37]):

$$\frac{1}{r} = b\frac{1}{R}, \tag{47}$$

with b of the order of magnitude about 1. According to [38], mean grain intercept λ for grain growth in Al is equal to $0.31r$. If one takes approximately that the mean grain intercept is half of grain diameter ($R = 1/2 \times 2R$), then, $b \approx 0.3$.

Combing above equations, we derive the following relation for dependence of the mean lateral grain size at the 'right' interface on the phase layer thickness:

$$\frac{dR}{d\Delta X} \approx b\frac{\gamma\Omega}{2kT}\frac{1}{R}. \tag{48}$$

If we approximate the initial condition as $R \approx 0$ at $\Delta X \approx 0$, then the integration of Eq. (48) gives the following parabolic dependence:

$$R^2 \approx 2b\frac{\gamma\Omega}{2kT}\Delta X, \quad R \approx \sqrt{b\frac{\gamma\Omega}{kT}\Delta X}. \tag{49}$$

Substitution of eq. (49) into eq. (37a) leads to the new time law of the IMC growth (which has never been predicted before but found experimentally).

$$\frac{d\Delta X^i}{dt} \approx \frac{\delta D^i_{GB}}{C^i(1-C^i)}\frac{1}{\sqrt{b\dfrac{\gamma\Omega}{kT}}}\frac{\Delta C^i}{(\Delta X^i)^{3/2}}, \tag{50}$$

so that

$$\Delta X^i \approx \frac{5\delta D^i_{GB}\Delta C^i}{2C^i(1-C^i)}\sqrt{\frac{kT}{b\gamma\Omega}}\cdot t^{2/5}. \tag{51a}$$

Thus, the time law for grain size will be

$$R \approx \sqrt{\sqrt{b\frac{g\Omega}{kT}}\frac{5d D^i_{GB}\Delta C^i}{2C^i(1-C^i)}\cdot t^{2/5}} \propto t^{1/5}. \tag{51b}$$

More rigorous version of this model is suggested in [33]. It takes into account that the lateral grain size is not the same along the IMC thickness, but it varies with IMC thickness and it is a descending function of x. If we take $x = 0$ at left boundary and $x = \Delta X^i$ at the right boundary, then,

$$R(x) \approx \sqrt{b\frac{\gamma\Omega}{kT}x}, \quad 0 < x < \Delta X. \tag{52}$$

In the steady state approximation, one gets [33]:

$$\frac{d\Delta X^i}{dt} \approx \frac{1}{C^i(1-C^i)}\frac{\delta\cdot D^{Wagner}_{GB}}{\dfrac{2}{3}\sqrt{b\dfrac{\gamma\Omega}{kT}}(\Delta X)^{3/2}}, \tag{53}$$

$$\Delta X^i \approx \frac{3}{2}\frac{5\delta D^i_{GB}\Delta C^i}{2C^i(1-C^i)}\sqrt{\frac{kT}{b\gamma\Omega}}\cdot t^{2/5}, \tag{54a}$$

$$R(x=\Delta X^i) \approx \sqrt{b\frac{\gamma\Omega}{kT}\Delta X^i} = \sqrt{\sqrt{b\frac{\gamma\Omega}{kT}}\frac{15\delta D^i_{GB}\Delta C^i}{4C^i(1-C^i)}}t^{1/5}. \tag{54b}$$

So, the only difference of this more rigorous approach, in comparison with Eqs. (51a, b), is the factor 3/2.

Thus, power laws for the intermetallic compound growth with time exponent 0.4 and the lateral grain growth with time exponent 0.2 are predicted. Direct experimental check of this prediction would be very interesting.

4.3. Reactions in Solid–Liquid Interactions

Now we come to reactions solid–liquid (actually, to soldering). Main references to our previous work can be found in [34–41].

After 2017, the two important new results were obtained in [42, 43]: (1) Extremely rapid grain growth in scallop-type Cu_6Sn_5 during solid–liquid interdiffusion reactions in microbump solder joint and (2) Ultrathin intermetallic compound formation in micro bump technology by the control of a low Zn concentration in solder.

4.3.1. Extremely Rapid Grain Growth in Scallop-Type Cu_6Sn_5 during Solid–Liquid Interdiffusion Reactions in Microbump Solder Joints

Modern packaging of microelectronic devices uses sandwich contacts copper–solder copper with solder thickness of 10 microns. Fast growth of Cu_6Sn_5 scallops during reflow from both sides arranges their meeting. After meeting, very fast, in a few seconds, the bamboo structure of Cu_6Sn_5 phase forms, which means very fast grain growth among Cu_6Sn_5 grains (Fig. 19).

In [42], we presented a simple model of this process. If the touching opposite scallops of Cu_6Sn_5 have close orientation, the may just merge, but in most cases one grain consumes another one due to fast transfer of atoms via thin liquid channels between grains. Existence of liquid channels is the consequence of wetting of the grain-boundaries between grains by the liquid solder. Velocity of both sides of the liquid channel between two grains is proportional to the product of copper mobility *via* liquid solder and the difference of chemical potential between neighbouring grains, and inversely proportional to the width of liquid channel:

$$V = \frac{1}{C_i - C^{melt}_{\mathrm{Cu}}}(\Omega J_{\mathrm{Cu}} - 0) = \frac{C^{melt}_{\mathrm{Cu}} D^{melt}_{\mathrm{Cu}}}{(C_i - C^{melt}_{\mathrm{Cu}})kT}\frac{\mu_2 - \mu_1}{\delta}\left[\frac{\mathrm{m}}{\mathrm{s}}\right]. \tag{55}$$

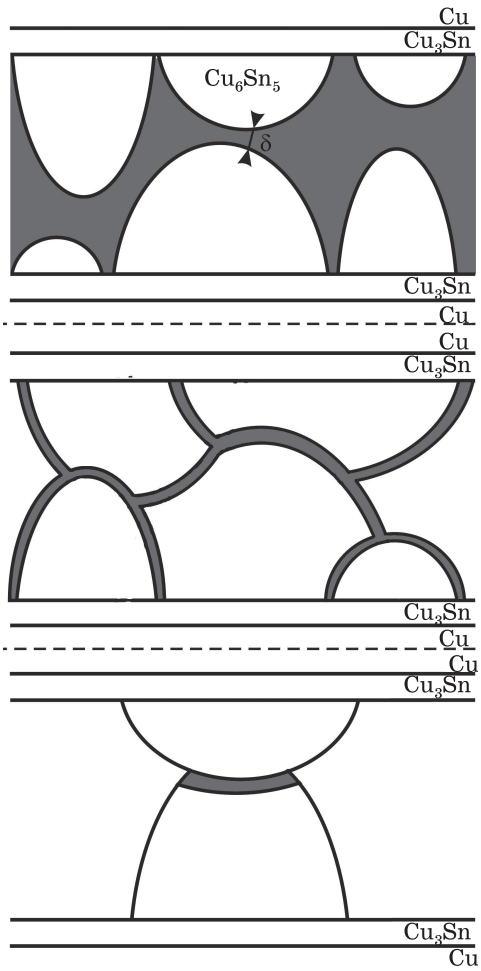

Fig. 19. Extremely rapid grain growth in scallop-type Cu_6Sn_5 during solid–liquid interdiffusion reactions in microbump solder joints

Difference between chemical potentials is determined by the Gibbs–Thomson potential, so that

$$V \approx \frac{4C_{\mathrm{Cu}}^{melt} D_{\mathrm{Cu}}^{melt}}{(C_i - C_{\mathrm{Cu}}^{melt})kT} \frac{\gamma_{\eta/melt}\Omega}{\delta \cdot R}. \qquad (56)$$

We managed also to estimate theoretically the width δ of channel:

$$\delta^* = \frac{\gamma_{\eta/\eta} - 2\gamma_{\eta/\mathrm{liquid}}}{\Delta g_{\varepsilon+\mathrm{solder}\to\eta}}\Omega. \qquad (57)$$

Taking reasonable values of main parameters,

$C_{\mathrm{Cu}}^{\eta} = \frac{6}{11}$, $C_{\mathrm{Cu}}^{melt} = 0.01$, $\gamma = 1\ \frac{\mathrm{J}}{\mathrm{m}^2}$,

$\Omega = 10^{-29}\ \frac{\mathrm{m}^3}{\mathrm{atom}}$, $D_{\mathrm{Cu}}^{melt} = 10^{-9}\ \frac{\mathrm{m}^2}{\mathrm{s}}$,

$R = 5 \cdot 10^{-6}$ m, $\delta = 1.5 \cdot 10^{-9}$ m,

$\gamma_{\eta/\eta} - 2\gamma_{\eta/\mathrm{liquid}} \approx 0.6\ \frac{\mathrm{J}}{\mathrm{m}^2}$,

$\Delta g_{\varepsilon+\mathrm{solder}\to\eta} \approx 0.4\ \frac{\mathrm{J}}{\mathrm{atom}}$, we get

$\delta^* \approx 1.5$ nm, $V = 7.5 \cdot 10^{-6}\ \frac{\mathrm{m}}{\mathrm{s}}$.

These values correspond to experimental data [42].

4.3.2. Ultra-Thin Intermetallic Compound Formation in Micro Bump Technology by the Control of a Low Zn Concentration in Solder

Another interesting phenomenological result is a simple model describing the influence of small addition of Zn to tin, on the kinetics and phase spectrum of soldering. Reaction between copper and liquid Sn–Zn–Bi–In solder containing low concentration of Zn was studied [43]. We found an extremely slow reaction rate with Cu substrate [43]. Other researchers have already found that the adding of Zn to Sn-based solder slows down the reaction kinetics and the phase spectrum of reaction

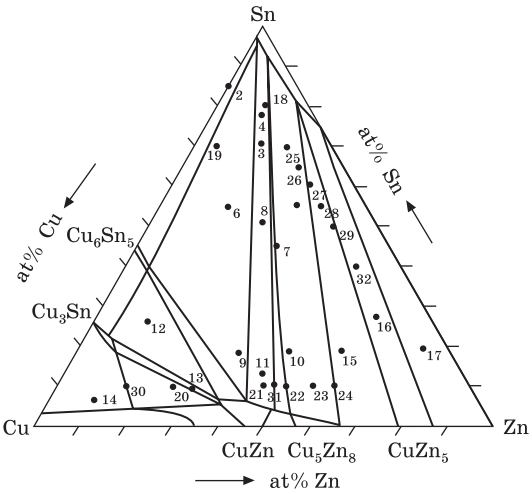

Fig. 20. Isothermal section of phase diagram Cu–Sn–Zn [44]

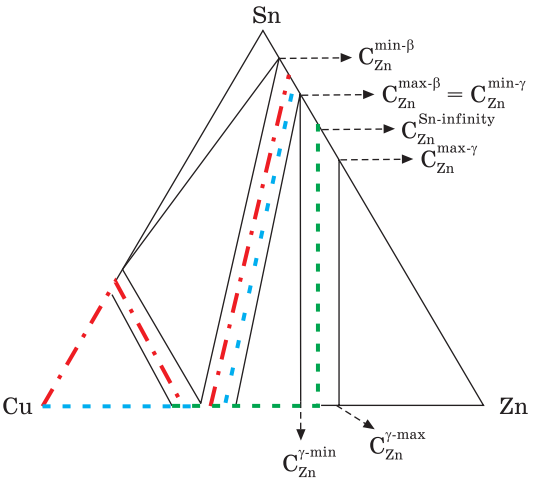

Fig. 21. Simplified phase diagram and alternative diffusion paths

zone. However, the IMC growth rate [43] was found to be much slower than usually. We developed a theoretical model for a systematic discussion of the competition among evolution paths in reactions between Cu with Sn–Zn solder. We explained that only a small amount of Zn can lead to the extremely slow reaction rate in IMC formation [43]. It is an important property for electronic packaging technology.

5-component system of Cu–Sn–Zn–Bi–In is too complicated for theoretical analysis. Because we treat mainly the formation of intermetallic phases on the basis of binary compounds of Cu_6Sn_5, CuZn, and Cu_5Zn_8, we simplify our analysis by considering the ternary system of Cu–Sn–Zn (Fig. 20), assuming that the role of Bi and In is in the reduction of eutectic temperature, but not the formation of new compounds in soldering reaction.

Even in this case, the situation with the choice of reaction path is complicated. At Fig. 21, you may see at least three possible alternative diffusion paths:

(a) Blue path, Cu–CuZn(*B*2-phase)–(Sn + Zn);

(b) Green path, Cu–CuZn(*B*2-phase)–Cu_5Zn_8(γ-phase)–(Sn + Zn);

(c) Red path, Cu–Cu_6Sn_5(η)–CuZn(β)–(Sn + Zn).

Please note that these paths do not demonstrate explicitly the shape of *S*-curve, predicted by Kirkaldy. Yet, it is not a mistake. Simply, in our case, one of the marginal phases of diffusion couple is liquid solder, diffusion in liquid is much faster than in solid part, so that the liquid section of the diffusion path in the concentration triangle (almost along

the tin–zinc side) is very short and tends just to point, coinciding with initial composition of liquid solder.

Moreover, some of intermediate phases along the indicated diffusion paths may be kinetically suppressed.

In the conditions described in [43], we found that the growing phase belongs to copper–zinc side and was close to gamma-phase.

We demonstrated that the growth rate is proportional to the cubic root of concentration difference between actual composition of zinc in solder, and the threshold composition in zinc, corresponding to ternary equilibrium between three phases: liquid solder, gamma-phase and beta-phase. In simplified case, when the grain size is proportional to the layer thickness, one gets:

$$\Delta X^{\gamma} = \left(\frac{C_{\mathrm{Zn}}^{\mathrm{Sn-infinity}} - C_{\mathrm{Zn}}^{\min-\gamma}}{C_{\mathrm{Zn}}^{\max-\gamma} - C_{\mathrm{Zn}}^{\min-\gamma}} \right)^{1/3} (12.6 \cdot \delta_{GB} D_{GB}^{\gamma} (C_{\mathrm{Zn}}^{\gamma-\max} - C_{\mathrm{Zn}}^{\gamma-\min})) t^{1/3}. \quad (58)$$

In more general case,

$$\Delta X = \left(\frac{8.4}{1-m} \frac{\mathrm{d}_{GB} D_{GB}^{\mathrm{g}}}{A} \frac{C_{\mathrm{Zn}}^{Sn-\mathrm{inf}inity} - C_{\mathrm{Zn}}^{\min-\mathrm{g}}}{C_{\mathrm{Zn}}^{\max-\mathrm{g}} - C_{\mathrm{Zn}}^{\min-\mathrm{g}}} (C_{\mathrm{Zn}}^{\mathrm{g}-\max} - C_{\mathrm{Zn}}^{\mathrm{g}-\min}) \right)^{1/2} t^{\frac{1-m}{2}}. \quad (59)$$

5. Main Conclusions

I. Recent stochastic modification of Kinetic Mean-Field, as well as Kinetic Monte Carlo, enables to model nucleation, simultaneous ordering and growth, and competition of the intermediate phases in solid-solid interactions, if one uses one of two tricks:

(a) Constant interaction energies within two coordination shells with opposite signs of mixing energies.

(b) Exponential dependence of interaction energy between two atoms on the local composition of the surrounding cluster.

II. Superposition law for Wagner diffusivity in multiphase reactive diffusion is found and proved: Interpenetration of components in parabolic regime of diffusion is proportional to the sum of Wagner diffusivities of all intermediate phases:

$$< (X - X_{Ma\tan o})^2 >= 2 \left(\int_0^{C_{\alpha}} \tilde{D}(C)\, dC + \sum_{k=1}^{n} \int_{(\Delta C(k))} \tilde{D}_k(C)\, dC + \int_{C_{\beta}}^{1} \tilde{D}(C)\, dC \right) t .$$

III. At low temperatures, when the interdiffusion proceeds mainly via grain-boundaries, the rate of lateral grain growth may be driven by interdiffusion flux, leading to time exponents 2/5 for phase thickness and 1/5 for lateral grain size.

IV. At the last stages of reaction in sandwich-like samples Cu–solder–Cu, the grains of Cu_6Sn_5 grow extremely fast, because they are

separated by liquid channels instead of usual grain boundaries, due to high diffusivity within liquid channels, and nanometric thickness of these channels.

V. Small addition of Zn to Sn may drastically change the phase spectrum of soldering as well as to slow down the reaction rate.

REFERENCES

1. K.-N. Tu, *Solder Joint Technology* (New York: Springer: 2007), p. 357; ISBN: 0-387-38890-7
2. F. Baras, V. Turlo, O. Politano, S.G. Vadchenko, A.S. Rogachev, A.S. Mukasyan, *Advanced Engineering Materials*, **20**, No. 8: 1800091 (2018); https://doi.org/10.1002/adem.201800091
3. S.Q. Arlington, S.V. Lakshman, S.C., Barron, J.B. DeLisio, J.C. Rodriguez, S. Narayanan, T.P. Weihs, *Materials Advances*, **1**, No. 5: 1151 (2020); https://doi.org/10.1039/D0MA00148A
4. El.M. Kousseifi, K. Hoummada, F. Panciera, C. Lavoie, D. Mangelinck, *Acta Materialia*, **198**: 100 (2020); https://doi.org/10.1016/j.actamat.2020.07.062
5. K.-N. Tu, A. M. Gusak, *Kinetics in Nanoscale Materials* (New York: John Wiley & Sons: 2014); ISBN: 978-0-470-88140-8
6. R. Chaim, Y. Amouyal, *Materials*, **12**, No. 9: 1494 (2019); https://doi.org/10.3390/ma12091494
7. A. Gusak, N. Storozhuk, *Diffusion-Controlled Phase Transformations in Open Systems. In Handbook of Solid State Diffusion* (Amsterdam, Netherlands: Elsevier: 2017), **Vol. 2**: pp. 37-100; https://doi.org/10.1016/B978-0-12-804548-0.00002-5
8. A.M. Gusak, T.V. Zaporozhets, Y.O. Lyashenko, S.V. Kornienko, M.O. Pasichnyy, A.S. Shirinyan, *Diffusion-Controlled Solid State Reactions: in Alloys, Thin Films and Nanosystems* (New York: John Wiley & Sons: 2010); ISBN: 978-3-527-40884-9
9. A.M. Gusak, O.Y. Lyashenko, F. Hodaj, *Inorganic Materials: Applied Research*, **10**, No. 3: 517 (2019); https://doi.org/10.1134/S2075113319030109
10. A.M. Gusak, *Ukrainian Journal of Physics*, **35**, No. 5: 725 (1990)
11. F. Hodaj, A.M. Gusak, P.J. Desre, *Philosophical Magazine A*, **77**, No 6: 1471 (1998); https://doi.org/10.1080/01418619808214264
12. A.M. Gusak, F. Hodaj, A.O. Bogatyrev, *Journal of Physics: Condensed matter*, **13**, No. 12: 2767 (2001); https://doi.org/10.1088/0953-8984/13/12/302
13. F. Hodaj, A.M. Gusak, *Acta materialia*, **52**, No. 14: 4305 (2004); https://doi.org/10.1016/j.actamat.2004.05.047
14. A.M. Gusak, F. Hodaj, G. Schmitz, *Philosophical Magazine Letters*, **91**, No. 9: 610 (2011); https://doi.org/10.1080/09500839.2011.600257
15. A.M. Gusak, A.O. Bogatyrev, A.O. Kovalchuk, S.V. Kornienko, Gr.V. Lucenko, Yu.A. Lyashenko, A.S. Shirinyan, T.V. Zaporoghets, *Progress in Physics of Metals,* **5**, No. 4: 433 (2004); https://doi.org/10.15407/ufm.05.04.433
16. G. Martin, *Physical Review B*, **41**, No. 4: 2279 (1990); https://doi.org/10.1103/PhysRevB.41.2279

17. Z. Erdelyi, D.L. Beke, A. Taranovskyy, *Applied Physics Letters*, **92**, No. 13: 133110 (2008); https://doi.org/10.1063/1.2905334
18. N.V. Storozhuk, K.V. Sopiga, A.M. Gusak, *Philosophical Magazine*, **93**, No. 16: 1999 (2013); https://doi.org/10.1080/14786435.2012.746793
19. Z. Erdelyi, M. Pasichnyy, V. Bezpalchuk, J.J. Toman, B. Gajdics, A.M. Gusak, *Computer Physics Communications*, **204**: 31 (2016); https://doi.org/10.1016/j.cpc.2016.03.003
20. V.M. Bezpalchuk, R. Kozubski, A.M. Gusak, *Progress in Physics of Metals*, **18**, No. 3.: 205 (2017); https://doi.org/10.15407/ufm.18.03.205
21. A. Gusak, T. Zaporozhets, *Metallofiz. Noveishie Tekhnol.*, **40**, No. 11: 1415 (2018); https://doi.org/10.15407/mfint.40.11.1415
22. A. Gusak, T. Zaporozhets, N. Storozhuk, *The Journal of Chemical Physics*, **150**, No. 17: 174109 (2019); https://doi.org/10.1063/1.5086046
23. T.V. Zaporozhets, A. Taranovskyy, G. Jager, A.M., Gusak, Z. Erdelyi, J.J. Toman, *Computational Materials Science*, **171**: 109251(2020); https://doi.org/10.1016/j.commatsci.2019.109251
24. A.G. Khachaturyan, Theory of Structural Transformations In Solids (New York: Dover Publications: 2013); ISBN: 0-486-46280-3
25. Y. Wang, L. Chen, A. Khachaturyan, *Solid-Solid Phase Transformation* (Warrendale, PA: TMS: 1994), p. 245; ISBN: 0-87339-278-7
26. A. Portavoce, G. Treglia, *Physical Review B*, **82**, No. 20: 205431 (2010); https://doi.org/10.1103/PhysRevB.82.205431
27. A. Portavoce, G. Treglia, *Physical Review B*, **85**, No. 22: 224101 (2012); https://doi.org/10.1103/PhysRevB.85.224101
28. C. Wagner, *Acta Metallurgica*, **17**, No. 2: 99 (1969); https://doi.org/10.1016/0001-6160(69)90131-X
29. A.M. Gusak, N.V. Storozhuk, *Metallofiz. Noveishie Tekhnol.*, **41**, No. 5: 583 (2019); https://doi.org/10.15407/mfint.41.05.0583
30. A.M. Gusak, M.V. Yarmolenko, *Journal of Applied Physics*, **73**, No. 10, 4881 (1993); https://doi.org/10.1063/1.353805
31. V.M. Pasichna, A.M. Gusak, *Cherkasy University Bulletin: Physical and Mathematical Sciences*, **1**: 9 (2019); https://doi.org/10.31651/2076-5851-2019-1-9-30
32. V. Pasichna, A. Gusak, *Computational Materials Science*, **187**: 110114 (2021); https://doi.org/10.1016/j.commatsci.2020.110114
33. A.M. Gusak, *Metallofiz. Noveishie Tekhnol.*, **42**, No. 10: 1335 (2020); https://doi.org/10.15407/mfint.42.10.1335
34. A.M., Gusak, K.-N. Tu, *Physical Review B*, **66**, No. 11: 115403 (2002); https://doi.org/10.1103/PhysRevB.66.115403
35. K.-N. Tu, A.M. Gusak, M. Li, *Journal of Applied Physics*, **93**, No. 3: 1335 (2003); https://doi.org/10.1063/1.1517165
36. J.O. Suh, K.-N. Tu, G.V. Lutsenko, A.M. Gusak, *Acta Materialia*, **56**, No. 5: 1075 (2008); https://doi.org/10.1016/j.actamat.2007.11.009
37. B.R., Patterson, Y. Liu, *Metallurgical Transactions A*, **23**, No. 9: 2481 (1992); https://doi.org/10.1007/BF02658051

38. O. Liashenko, A.M. Gusak, F. Hodaj, *Journal of Materials Science*: *Materials in Electronics*, **25**, No. 10: 4664 (2014); https://doi.org/10.1007/s10854-014-2221-7
39. F. Hodaj, O. Liashenko, A.M. Gusak, *Philosophical Magazine Letters*, **94**, No. 4: 217 (2014): https://doi.org/10.1080/09500839.2014.886782
40. A. Gusak, F. Hodaj, O. Liashenko, *Philosophical Magazine Letters*, **95**, No. 2: 110 (2015); https://doi.org/10.1080/09500839.2015.1020350
41. A.M. Gusak, C. Chen, K.-N. Tu, *Philosophical Magazine*, **96**, No. 13: 1318 (2016); https://doi.org/10.1080/14786435.2016.1162913
42. A.M. Gusak, K.-N. Tu, C. Chen, *Scripta Materialia*, **179**: 45 (2020); https://doi.org/10.1016/j.scriptamat.2020.01.005
43. Y. Liu, L. Pu, A. Gusak, X. Zhao, C. Tan, K.-N. Tu, *Materialia*, **12**: 100791 (2020); https://doi.org/10.1016/j.mtla.2020.100791
44. C.Y. Chou and S.W. Chen, *Acta Materialia*, 54, No. 9: 2393 (2006); https://doi.org/10.1016/j.actamat.2006.01.014

Received 19.08.2021;
in final version, 02.11.2021

А.М. Гусак, Н.В. Сторожук
Черкаський національний університет імені Богдана Хмельницького, бульв. Шевченка, 81, 18031 Черкаси, Україна

МОДЕЛЮВАННЯ ФАЗОУТВОРЕННЯ У ПРОЦЕСАХ ТВЕРДО-ТВЕРДОФАЗНОЇ ТА ТВЕРДО-РІДКОФАЗНОЇ ВЗАЄМОДІЇ: НОВІ РЕЗУЛЬТАТИ

Розглядаються нові результати, одержані після 2016 року в галузі моделювання фазоутворення за твердо-твердофазних і твердо-рідкофазних реакцій методами СКСП (стохастичний кінетичний середньо-польовий), Монте-Карло та феноменологічним. Правдоподібні результати моделювання реакційної багатофазної дифузії, зокрема утворення чітких концентраційних плато для кожної впорядкованої проміжної фази та чітких концентраційних перепадів між ними одержуються методами СКСП та Монте-Карло, якщо в моделі врахувати міжатомні взаємодії в другій координаційній сфері так, що енергія змішання в першій сфері — від'ємна, а в другій — додатна. Іншою можливістю одержати правдоподібні результати моделювання реакційної дифузії є використання міжатомних взаємодій, залежних від локального хімічного складу, із максимумами для стехіометричних концентрацій. У феноменологічному моделюванні вводяться узагальнення концепції коефіцієнта взаємної дифузії за Ваґнером і відповідне правило суперпозиції. Запропоновано новий механізм латерального росту зерен у зростаючих прошарках проміжних фаз під час реакційної дифузії. Повідомляється про відкриття аномально швидкого росту зерен на фінальній стадії паяння контактів «сандвічевого» типу мідь–цина–мідь і про теорію цього явища. Також описано просту модель врахування впливу добавок Цинку на реакцію мідь–цина.

Ключові слова: взаємна дифузія, проміжні фази, впорядкування, моделювання, середньо-польове наближення, шум, метод Монте-Карло, паяння